Article

Synthesis and Characteristics of a Fish Scale-Based Biochar–Nanosilver Antibacterial Material

Zhichao Zhang [1,2] and Yucai He [1,*]

1   School of Pharmacy, Changzhou University, Changzhou 213164, China; zhangzhichao9088@163.com
2   School of Chemistry and Chemical Engineering, Guangxi University, Nanning 530004, China
*   Correspondence: heyucai2001@163.com

Abstract: Microbial contamination has caused various diseases via pathogenic bacteria, endangering people's lives every day. Recently, increasing attention has been paid to the exploration of new and effective antibacterial materials. In this paper, we attempted to synthesize a fish scale charcoal nanosilver antibacterial composite using waste fish scale as a carbon substrate. X-ray diffraction, Fourier-transform infrared spectroscopy, thermogravimetry-differential scanning calorimetry, and scanning electron microscopy showed that the structure of the nanosilver fish scale material formed and the nanosilver particles formed account for 72.1% of the silver element. Its antibacterial ability against *Escherichia coli*, *Staphylococcus aureus*, and *Pseudomonas aeruginosa* was examined using the plate counting method and inhibition zones; the maximum inhibition zone was 32 mm. The antibacterial rate could reach >99.9%, indicating that this prepared material had excellent antibacterial activity. After 20 batches of bacteriostasis, the bacteriostasis rate was more than 90%, indicating that the fish scale/silver composite had sustained antibacterial ability and excellent antibacterial reusability. Finally, potential antibacterial mechanism was proposed. Overall, the fish scale/silver composite has a good application prospect and a wide range of applications in the handling of microbial pollution in the future.

Keywords: waste fish scale; nanosilver antibacterial composite; antibacterial ability; antibacterial reusability; microbial pollution

1. Introduction

It is well known that sewage causes many diseases and harms humans, plants and animals and thus needs to be dealt with in a timely manner [1]. Currently, the most general method is to use filtration equipment that causes significant economic losses. However, most researchers focus on the ability of the filter capacity, and ignore the bacteriostatic properties of the filter material. Sewage is an excellent breeding ground for microorganisms, and most disease-causing bacteria grow in this wet environment of the sewage, which lead to bacteria growth on many filtration materials [2]. If the filter is not thoroughly disinfected, the residual pathogenic bacteria would harm people's health [3], and cause the decline of people's resistance and even lead to death [4,5]. Hence, researchers are increasingly trying to reduce microbial pollution in sewage [6,7].

For a series of microbial contamination problems, antibacterial materials have been widely studied by researchers [8]. Focus is largely on preparing metal ion antibacterial materials due to their high efficiency and simplicity [9]. Among many metal ions, silver is often utilized in antibacterial composites due to its good biocompatibility and durability [10]. Silver nanoparticles (AgNPs) can be applied to damage cell membranes; they also enter cells directly, quickly combine with mercaptan in oxygen metabolism, and block metabolism [11,12]. Antibacterial complex composed of Ag/C has good germicidal efficacy against *E. coli*, *P. aeruginosa* and *S. aureus* [13]. Silver ions are widely used in the preparation of biochar antibacterial materials, which show excellent antibacterial effects and good

application prospects [14]. The biochars are ubiquitous and have the attractive advantages of large specific surface area, cost effectiveness, good adsorption capacity, and excellent thermostability [15–20]. The preparation of environmentally friendly silver nanoparticles antibacterial materials has gained widespread attention in the utilization of biobased materials [21].

It is known that fish produce a lot of waste during processing; ~80 million tons of fish wastes are produced globally each year [22]. Fish are rich in protein, calcium, vitamins, fat and minerals [23–25]. However, fish waste is dangerous, and its handling produces high chemical oxygen demand (COD), and biological oxygen demand (BOD) and it also contains some pathogenic microorganisms [26]. Thus, it is necessary to develop effective strategies for the management of fish waste [27]. To date, fish scale waste has been widely exploited and applied as multifunctional biobased materials [28]. In some studies, biological-based coatings of ichthyrin and phytic acid have been used for flame-retardant cotton fabrics [29]. Fish scale gelatin was extracted from waste fish scale and used to make active food packaging [30,31]. It is also widely used in medical body stents [32,33]. However, there are just a few reports on waste fish scales as antibacterial materials. Only fish scale gelatin films have been reported in some studies [34,35]. A wide array of studies is focused on the efficient utilization of waste [36–39].

In this paper, fish scales biochar and silver nitrate were used to synthesize the composites with antibacterial properties. This composite was characterized via X-ray diffraction, Fourier-transform infrared spectroscopy, thermogravimetry-differential scanning calorimetry, and scanning electron microscopy. Antibacterial tests of the fish-scale/Ag composite were conducted against *E. coli*, *P. aeruginosa* and *S. aureus*. The preparation method, calcination temperature, and silver loading concentration of the composite were optimized. The antibacterial property and durability of the composite were also examined.

2. Materials and Methods

2.1. Chemicals and Bacteria

Silver nitrate (Silver nitrate $\geq$ 99.8%), sodium chloride (NaCl $\geq$ 99.5%) and sodium citrate dihydrate ($C_6H_5Na_3O_7 \cdot 2H_2O \geq$ 99.0%) were bought from Runyou Reagents Co., (Changzhou, China). Yeast powder, tryptone and agar were obtained from Oxoid (Shanghai, China). Waste fish scales were obtained from Zhongshui Product Store in an aquatic product market on Daming Road, Nanjing, China. *E. coli* ATCC 25922, *P. aeruginosa* ATCC 27853 and *S. aureus* ATCC 6538 were bought from the Microbiology Institute of Shanghai in China.

2.2. Preparation of the Antibacterial Material

Firstly, fresh grass scales were soaked in water for 30 min to loosen the adherent skin, and they were washed thoroughly with tap water three times to remove dirt and water-soluble impurities, then they were boiled, and then further impurities were removed with clean water. Then, waste fish scales were dried in a 70 °C oven until scales became brittle and reached a constant weight. Secondly, the dried fish scales were calcined in the muffle furnace at 300 °C for 2 h to carbonize them, and then removed after cooling for grinding. Briefly, 5 g carbonized fish scale powder was added into 100 mL silver nitrate (0.5 g/L) solution and stirred for 2 h. Thirdly, the above solution was then added to sodium citrate dihydrate (0.2 g) for reducing silver ions and then soaked for 24 h, filtered and dried. Fourthly, the dried powder was taken out, grounded, crushed, and calcined again. Then, the complexes were placed in crucibles and were put in a muffle furnace, which was gradually heated to the designed temperatures (150, 200, 250, 300, 350, 400, and 500 °C) in a heating speed of 10 °C per minute; the treatment was kept under the highest temperature for 2 h. Until the muffle oven was cooled down to room temperature, the fish scale mixture F/C–Ag was taken out and milled to powders. The F/C–Ag composite is silver-loaded

at a temperature of 250 °C, denoted as F/C–Ag$_{250}$. The yield of silver-carrying fish scale biochar was calculated using the following formula:

$$Y = X/Z$$

X is the low-temperature carbonation quality of fish scales. Z is the mass of fish scales before calcination. Y is the yield of bacteriostatic material.

2.3. Antibacterial Testing

E. coli ATCC 25922, *P. aeruginosa* ATCC 27853 and *S. aureus* ATCC 6538 were used in this bacteriostatic experiment. Before the experiment, all glassware and experimental materials were sterilized in an autoclave (20 min, 121 °C). The disposable Petri dishes were sterilized via UV for 20 min in an ultra-clean table before use. The bacteriostatic test was observed via diffusion and plate counting [40].

In the diffusion method, 100 μL bacterial suspension (*S. aureus*, *P. aeruginosa*, and *E. coli*) was evenly coated on the agar LB solid medium with 9 mm holes [41]. Briefly, 0.1 g F/C–Ag was then added to the well and incubated at 37 °C for 24 h; bacterial growth around the material was observed [42].

In the plate counting method, 100 μL bacterial suspension (*S. aureus*, *P. aeruginosa*, and *E. coli*) were grown on the agar LB solid medium (37 °C) for 1 day. The antibacterial rate (AR) was defined as below:

$$Antibacterial\,rate(\%) = (A1 - A2)/A1 \times 100$$

A1 is the number of untreated colonies, and A2 is the number of colonies treated with F/C–Ag.

2.4. Optimization of the Preparation Method of the F/C–Ag Composite

The carbon of fish scale was denoted as blank A. The fish scale carbon was soaked overnight in 0.5 g/L silver nitrate solution, then removed, filtered and dried as method B. The fish scale carbon was reduced and soaked overnight in 0.5 g/L silver nitrate solution with sodium citrate dihydrate, and was taken out, filtered and dried as method C. The fish scale carbon was soaked overnight in 0.5 g/L of silver nitrate solution, and was taken out, filtered and dried for secondary calcination as method D. The fish scale carbon was reduced and soaked overnight in 0.5 g/L silver nitrate solution with sodium citrate dihydrate, and was taken out, filtered and dried for secondary calcination as method E.

Briefly, 100 μL bacterial suspension (*S. aureus*, *P. aeruginosa*, and *E. coli*) with initial concentration of 10^8 CFU/mL was uniformly coated in solid medium. The holes were drilled in the agar medium using a hole puncher. The composite materials (B, C, D, and E) were added to the holes and A was utilized as a control test cultivation at 37 °C for 24 h; *E. coli* growth was observed around the material. The bacteriostasis test was repeated three times to check the reproducibility of the results.

2.5. Optimization of Silver Nitrate Concentration of the F/C–Ag Composite

The 100 μL bacterial suspension was uniformly coated on the solid LB medium with 9 mm holes and 0.1 g F/C–Ag prepared with different concentrations of silver nitrate (0.01, 0.1, 0.5, 1, 2, and 4 g/L) was added. After incubation at 37 °C for 24 h, the size of the antibacterial zone was measured.

2.6. Dosage and Time Optimization of the F/C–Ag Composite

S. aureus, *P. aeruginosa*, and *E. coli* were used as a standard for the dose and time optimization experiments. According to the plate counting method [40], the bacterial suspension was 10^8 CFU/mL. The loading of F/C–Ag composite were 0.2, 0.4, 0.6, 0.8 and 1.0 g/L.

The bacterial suspension was mixed and cultured in a 37 °C thermostatic oscillator. The bacterial suspension (*S. aureus*, *P. aeruginosa*, or *E. coli*) was incubated for 1, 3, 5, 7, and 9 h after the addition of antibacterial substances; 100 μL bacterial suspension was taken out and diluted with 0.9% normal saline for a certain number of times until the plate counting method was available.

2.7. Minimum Inhibitory Concentration

Using *S. aureus*, *P. aeruginosa*, and *E. coli* as standard bacteria, the minimum inhibitory concentration of the F/C–Ag composite was determined using the double gradient dilution method [43–45]. An appropriate amount of F powder was accurately weighed and was dissolved in sterile water to form a solution with a certain concentration. The minimum inhibitory concentration of F/C–Ag was determined using the double gradient dilution method and gradient dilution was performed with sterile distilled water. *S. aureus*, *P. aeruginosa*, and *E. coli* were grown to logarithmic phase and diluted to 10^5 CFU/mL using the gradient with LB medium. Briefly, 1 mL of the bacterial solution was put into sterile 4 mL centrifuge tubes numbered 2 to 10, and the pre-diluted bacterial solution was added to each centrifuge tube. In the first centrifuge tube, 1 mL diluted bacterial solution and 1 mL sterile water were added as blank control. The above process was completed within 15 min and two parallel processes were performed. After mixing, the centrifuge tube was placed in an oscillator for 18 h at 37 °C. After taking it out, it was beaten and OD_{600} was determined vias ultraviolet spectrophotometer [43–45]. F/C–Ag concentration was taken as the abscissa, OD_{600} value as the ordinate, and the inflection point was the minimum inhibitory concentration.

2.8. Antibacterial Reusability

The reuse performance of the F/C–Ag composite material is also very important in practical application [46]. Three kinds of bacteria (*S. aureus*, *P. aeruginosa*, and *E. coli*) were tested separately in water. After the completion of the first test, the centrifuge was rotated at 8000 rpm for 3 min, and the mixture was withdrawn, and further washed with sterile water for 3 times, followed by the next test cycle. In the bacteriostatic experiment of *P. aeruginosa*, the original bacteriostatic performance was still maintained after 20 times of repeated use. In the bacteriostatic experiment of *E. coli*, the bacteriostatic performance decreased slightly after 14 times of repeated use, and the bacteriostatic effect remained 95% after 20 times of repeated use. In the antibacterial experiment of *S. aureus*, after 8 times of repeated use, the antibacterial performance began to decline and stabilized at 20 times.

2.9. Characterization of the F/C–Ag Composite

A Fourier-transform infrared spectrometer (FT-IR) (Nicolet iS50 Thermo Scientific Co., Waltham, MA, USA) in the range of 500 cm^{-1} to 4000 cm^{-1} was utilized to analyze the antibacterial material. A scanning electron microscope (SEM) (Zeiss Sigma 300, Jena, Germany) was used to observe the surface morphology of the composite materials. Brunauer–Emmett–Teller (BET) (Micromeritics ASAP 2460, Waltham, MA, USA) surface area obtained via N_2 adsorption was adopted to characterize the specific surface area for the porous F/C–Ag composite. The binding state and crystal structure of the antibacterial material were analyzed using X-ray diffraction (XRD) (Smart Lab SE, Tokyo, Japan) over 10–80°. The valence changes of Ag ions in the complex were analyzed via X-ray photoelectron spectroscopy (XPS) (Thermo Kalpha, Waltham, MA, USA). The curves of mass and temperature or time and the stability of antibacterial material were studied using TG-DSC (TGA5500, New Castle, DE, USA).

3. Result and Discussion
3.1. Characterization of the F/C–Ag Composite

After detection via FT-IR, different functional groups could be identified based on the characteristic bonds, as displayed in Figure 1. The characteristic peak at 1625 cm^{-1} in the

silver-loaded fish scale biochar belonged to the absorption of carboxylic acid groups [41]. The characteristic peak at 1592 cm^{-1} was the deformation vibration of N-H [47]. The peak located at 1401 cm^{-1} was generated by carbonate ions [23], which were slightly smaller in the fish scale carbon due to the pyrolysis of calcium carbonate in the calcined fish scale. The C-C stretching vibration absorption peak was located at 1353 cm^{-1} [11]. The peak near 1101 cm^{-1} was associated with the C-O tensile vibration [48]; the tensile vibration of hydroxyapatite was significantly larger than that of the fish scale biochar material and the initial fish scale. The characteristic peak of HPO_4^{2-} in fish scale biochar materials and hydroxyapatite materials was located at 875 cm^{-1} [48]; the peak of hydroxyapatite was slightly larger than that of fish scale biochar. The initial fish scale did not show the characteristic peak of HPO_4^{2-}. A weak absorption peak of C-H bending vibration was found at 760 cm^{-1}. Curve G showed no C-H bending vibration at 760 cm^{-1}. The absorption peak at 610 cm^{-1} was generated by the rotation of the hydroxyl group [49]. Peaks of PO_4^{3-} appeared near 565 cm^{-1} and 1026 cm^{-1}. After the calcination of fish scales, the area of PO_4^{3-} peak increased obviously, and hydroxyapatite formed [49].
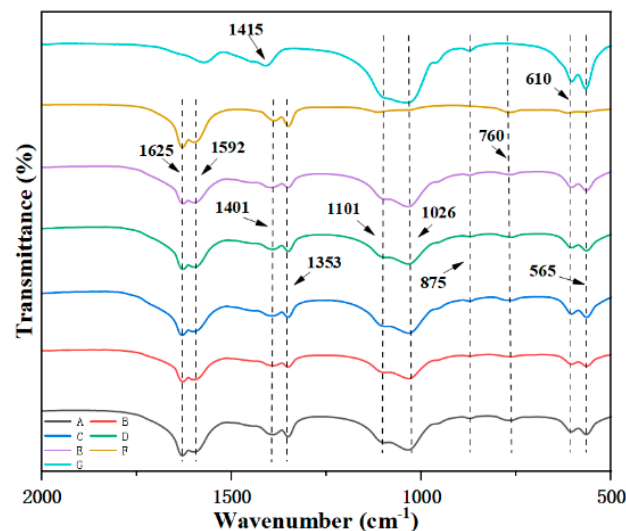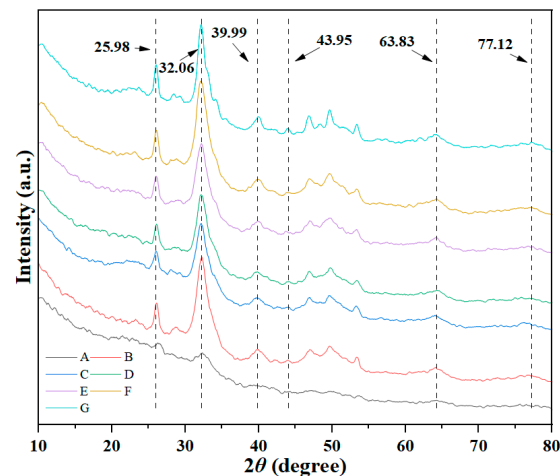

Figure 1. FT-IR images of fish scale biochar (**A**), non-reductive drying of silver ions (**B**), silver ion reduction drying (**C**), non-reductive calcination of silver ions (**D**), silver ion reduction calcination (**E**), fish scale (**F**), and hydroxyapatite (**G**).

Figure 2 displayed the XRD patterns of different fish scale biochar antibacterial materials (B, C, D, E, and F) and fish scale and hydroxyapatite antibacterial materials. The diffraction peaks (2θ) at 39.99°, 43.95°, 63.83°, and 77.12° were ascribed to the Ag element [47], verifying that silver ions are reduced to silver nanoparticles upon contact with sodium citrate dihydrate and in the subsequent carbonization process. Figure 2 illustrated that the diffraction peaks of hydroxyapatite in different fish scale biochar antibacterial materials were 2θ = 25.98° and 2θ = 32.6°, respectively. By comparing the original fish scales and hydroxyapatite antibacterial materials, we see that the antibacterial material of the treated fish scale biochar corresponded exactly to hydroxyapatite, which was the substance in the fish scale [48].

SEM was utilized to measure the F/C–Ag composite (Figure 3). The fish scale biochar from (Figure 3a,b) was calcined at low temperature, showing a fragmented and massive structure. When these samples were observed under the magnification of 3000 and 5000 times (Figure 3c,d), some nanosilver and corresponding clusters were attached to the surface of the F/C–Ag composite. The SEM was further scaled up to 10,000 and 30,000 times (Figure 3e,f). Silver nanoparticles were uniformly attached to the surface of the composite. In the process of production, nanosilver particles were obtained by adding the mixture of sodium citrate and water to reduce silver ions, and then nanosilver was fixed via low-temperature calcination. The surface area changes of fish scale and the F/C–Ag composite

were tested via BET, and the results are displayed in Table S1 (in Support Information). Fish scale had a small specific surface area (11.9 m^2/g), big pore volume (0.02 cm^3/g) and large pore size (13.4 nm). After calcination and silver attachment, the specific surface area increased to 45.6 m^2/g, while small pore volume (0.01 cm^3/g) and pore size (5.1 nm) were obtained.

Figure 2. XRD images of fish scale biochar (**A**), non-reductive drying of silver ions (**B**), silver ion reduction drying (**C**), non-reductive calcination of silver ions (**D**), silver ion reduction calcination (**E**), fish scale (**F**), and hydroxyapatite (**G**).
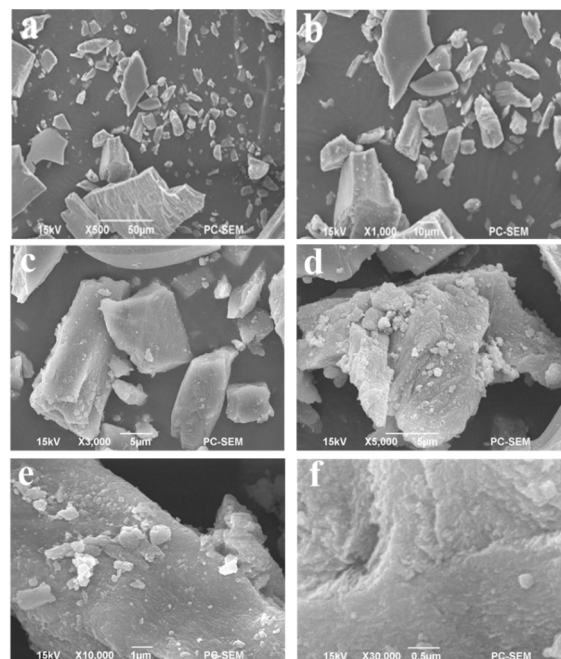

Figure 3. SEM images of F/C–Ag, 500 magnification (**a**), 1000 magnification (**b**), 3000 magnification (**c**), 5000 magnification (**d**), 10000 magnification (**e**), and 30,000 magnification (**f**).

XPS was employed to analyze the fish scale-based bacteriological materials prepared in four ways, and the results are displayed in Figure 4. For method A, the binding energy positions of silver elements were 367.6 eV and 373.6 eV corresponding to Ag^{1+} 3d$_{5/2}$ and Ag^{1+} 3d$_{3/2}$, respectively, accounting for 27.9%; 368.4 eV and 374.4 eV were attributed to Ag(Metal)3d$_{5/2}$ and Ag(Metal)3d$_{3/2}$ [50], respectively, which accounted for 72.1%. For method B, 367.7 eV and 373.7 eV were ascribed to Ag^{1+}3d$_{5/2}$ and Ag^{1+}3d$_{3/2}$, respectively, accounting for 37.2%; 368.4 eV and 374.3 eV were associated with Ag(Metal)3d$_{5/2}$ and

Ag(Metal)$3d_{3/2}$ [51], respectively, accounting for 63.8%. For method C, the electron binding energy position of silver element was 367.6 eV and 373.6 eV corresponding to Ag$^{1+}3d_{5/2}$ and Ag$^{1+}3d_{3/2}$, respectively, which accounted for 39.0%; 368.4 eV and 374.1 eV were ascribed to Ag(Metal)$3d_{5/2}$ and Ag(Metal)$3d_{3/2}$ [52], respectively, accounting for 61.0%. For method D, the electron binding energy position of silver element was 367.6 eV and 373.6 eV corresponding to Ag$^{1+}3d_{5/2}$ and Ag$^{1+}3d_{3/2}$, respectively, accounting for 54.7%; 368.4 eV and 373.9 eV were associated with Ag(Metal)$3d_{5/2}$ and Ag(Metal)$3d_{3/2}$ [53], respectively, accounting for 45.3%. From the analysis of Figure 4, it could be seen that most silver elements were generated when method A was used. The results of XPS analysis corresponded to the antibacterial test. It was thus proven that low-temperature calcination after reduction in sodium citrate dihydrate was beneficial to form more silver elements.
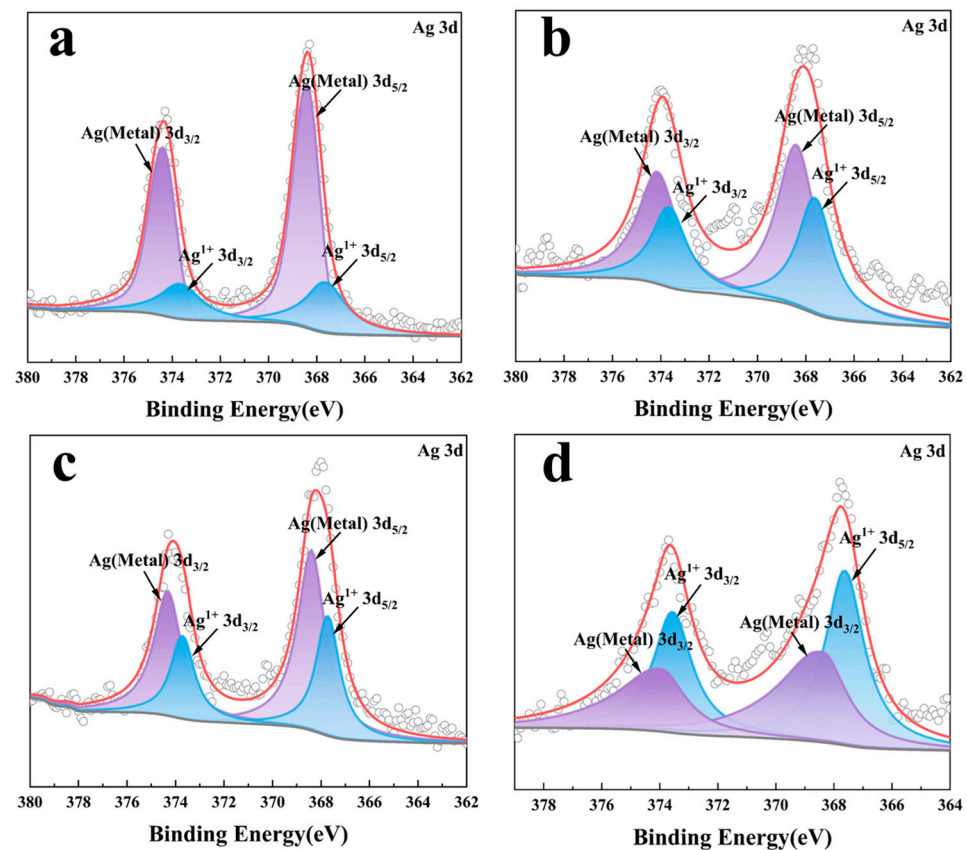

Figure 4. XPS images of silver ion reduction calcination (**a**), silver ion reduction drying (**b**), non-reductive calcination of silver ions (**c**), and non-reductive drying of silver ions (**d**).

Figure 5 displayed the TG curves of fish scale carbon, fish scale and the F/C–Ag composites under different processes and hydroxyapatite antibacterial materials in the temperature range of 50–800 °C. As could be seen from the TG curve in Figure 5, except for one weight loss platform for the hydroxyapatite bacteriostatic material, there were only two weight loss platforms for fish scale, fish scale biochar and fish scale-based bacteriostatic materials with different production processes. It was observed that there were two stages of fish scale biochar weight loss, as displayed in Figure 5a. The first stage of weight loss was about 5% at 50–160 °C, mainly due to the evaporation of water [11]. The second stage of weight loss was at 390–800 °C [49], which was about 20%, mainly due to the decomposition of residual protein, fat, organic calcium and hydroxyapatite in fish scale biochar with the increase in temperature. The weight loss of fish scale-based bacteriostatic materials produced via different processes had two stages, as illustrated in Figure 5b–e. The first stage of weight loss was about 4~6% at 50–180 °C, mainly due to the evaporation of water [12]. The second stage of weight loss was about 24–27% at 370–800 °C, which was mainly

due to the decomposition of sodium citrate dihydrate in fish scale-based bacteriostatic material, residual proteins, fats, organic calcium and hydroxyapatite with the increase in temperature [49]. There are two stages of weight loss in fish scales, as presented in Figure 5f. The first stage of weight loss was about 9% at 50–220 °C, due to loss of water in the sample. The second stage of weight loss was about 45% at 260–740 °C, which was mainly due to the gradual rise in temperature. When the temperature reached the melting point of protein, protein would lose most of its weight due to thermal decomposition and volatilization. There was only one stage of weight loss of the hydroxyapatite, as shown in Figure 5g. The weight loss is about 8% at 50–800 °C, caused with the increase in temperature, due to the decomposition of hydroxyapatite. The results of TG showed that this prepared F/C–Ag material had excellent stability at 400 °C. The thermogravimetric results of the F/C–Ag material were consistent with the general thermostability of antibacterial materials [54].
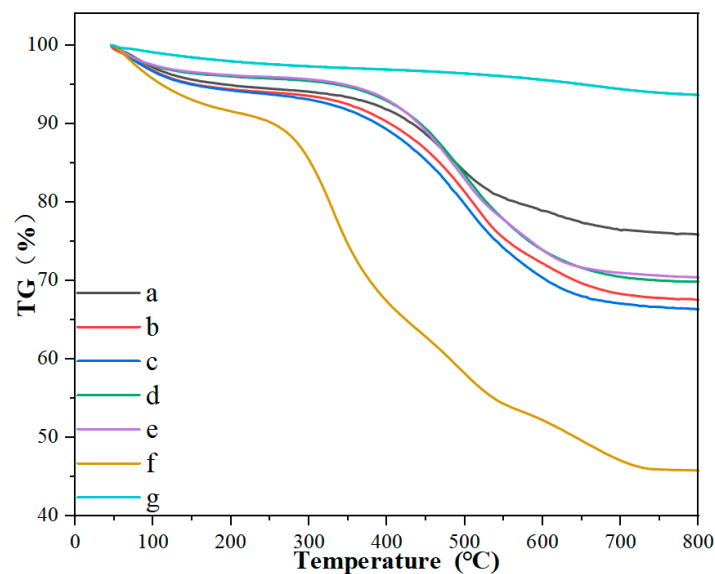

Figure 5. TG images of fish scale biochar (**a**), non-reductive drying of silver ions (**b**), silver ion reduction drying (**c**), non-reductive calcination of silver ions (**d**), silver ion reduction calcination (**e**), fish scale (**f**) and hydroxyapatite (**g**).

3.2. Antibacterial Property

3.2.1. Effect of the Production Method

The bacteriostatic material of silver ion reduction calcination might influence the bacteriostatic effect [55]. Figure 6 revealed that fish scale biochar without any treatment had no bacteriostatic effect. The bacteriostatic material of silver ion reduction calcination had obvious bacteriostatic effect on the three kinds of bacteria compared to the other different processes. By comparing the antibacterial zone sizes of the three bacteria, the F/C–Ag composite material had the best effect on *P. aeruginosa*, followed by *E. coli*, and *S. aureus*. The traditional nanosilver antibacterial material showed antibacterial activity against *E. coli*, *S. aureus*, and *P. aeruginosa* [56,57], and the antibacterial ability was similar to that of the F/C–Ag composite. The results of XPS indicated that the yield of silver was the highest under the silver ion reduction calcination process. Therefore, the F/C–Ag composite adopted the optimal process of silver ion reduction calcination.
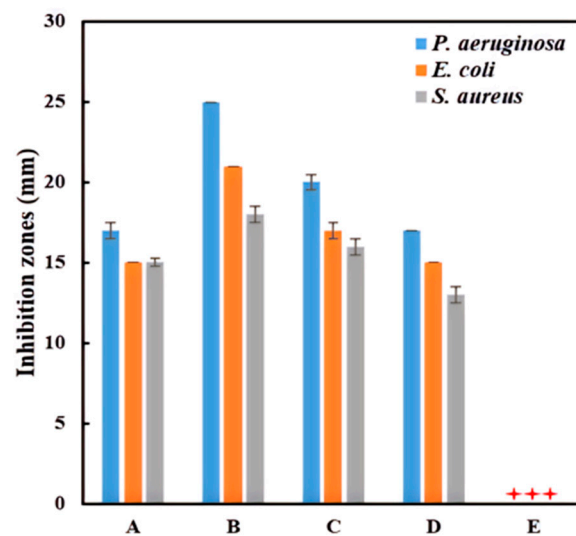
Figure 6. Antibacterial effect of fish scale biochar (**A**), silver ion reduction drying (**B**), silver ion reduction calcination (**C**), non-reductive calcination of silver ions (**D**), non-reductive drying of silver ions (**E**). ©+++ no antibacterial effect.

3.2.2. Effect of Calcination Temperature

The calcination temperature might influence the antibacterial effect [47], and the results are given in Figure 7. When the calcination temperature was between 250 and 500 °C, the antibacterial effect of the F/C–Ag composite material decreased. This shows that the bacterial inhibitory activity of F/C–Ag dropped after calcination at 250 °C for 2 h. The calcination temperature would influence the antibacterial property of nanoparticles, and the antibacterial activity might drop with increasing calcination temperature [58].
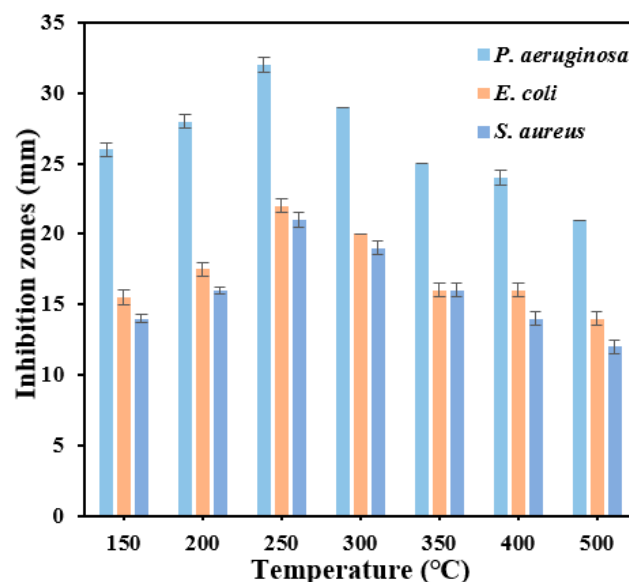

Figure 7. Effect of the F/C–Ag composites on bacteriostatic effects of *E. coli*, *P. eruginosa* and *S. aureus* at different calcination temperatures.

Thus, considering the influence of bacteriostatic effect of fish scale-based bacteriostatic material, 250 °C was selected as the appropriate carbonation temperature.

3.2.3. Effect of Silver Ion

At low silver ion concentrations, the inhibition zone size might be improved with the increase in silver ion dosage [59]. Figure 8 depicted that the bacteriostatic effect

became more obvious with the increase in silver nitrate dosage in the range of 0.05–0.5 g/L under the optimal production process. When the concentration of silver nitrate was in the range of 0.5–4.0 g/L, the bacteriostatic effect dropped with the increasing concentration of silver nitrate. In other word the bacteriostatic effect decreased with the increase in silver nitrate concentration. In the process of silver ion reduction by adding sodium citrate dihydrate, high silver ion concentration would cause the aggregation of silver ion functional groups [60]. Silver ions could not be uniformly attached to the surface of fish scale biochar, which led to the reduction and stabilization of the antibacterial effect when silver nitrate dose was increased. When silver nitrate was 0.5 g/L, the size of the microbial inhibition zone of the silver-loaded carbon was 18 mm [56], while the antibacterial zone of the F/C–Ag material reached more than 30 mm. Thus, the F/C–Ag material had good antibacterial activity.
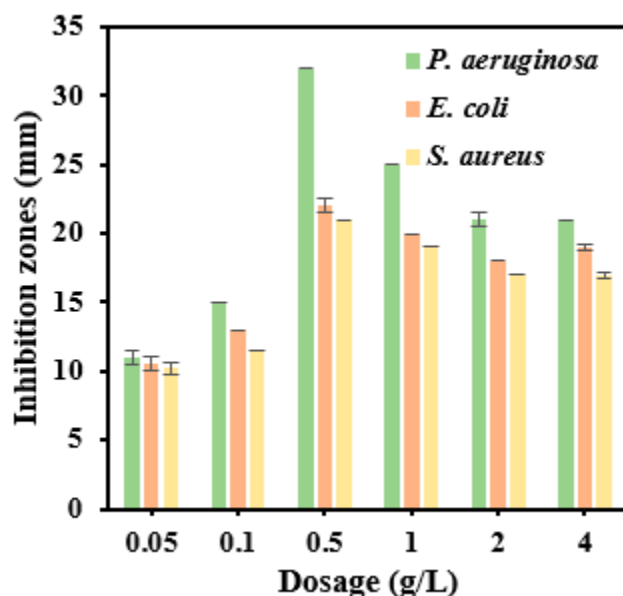

Figure 8. Effect of F/C–Ag composites on bacteriostatic effects at different concentrations of silver ions.

3.2.4. Effects of the F/C–Ag Composite Dosage and Treatment Time

The dosage and time of antibacterial material will have important influence on the antibacterial result [12]. With the increase in the amount of material and the time of release, the antibacterial effect might be enhanced. Figure 9 illustrated that with the change in bacteriostatic time and the increase in the F/C–Ag composite dosage, the bacteriostatic effect also changed significantly. The F/C–Ag composite material had significant antibacterial effect in the antibacterial experiment of *E. coli* (Figure 9a). In the treatment with the F/C–Ag composite (0.2 g/L) for 1 h, the antibacterial effect was 99.8%. When the concentration increased to 0.4 g/L and the inhibition time was 1 h, no colonies could be seen through the plate counting method. As the concentration continued to rise to 1 g/L, no remnant colonies were visible via plate counting. When the concentration of the F/C–Ag composite material was 0.2 g/L and the bacteriostatic time was 3 h, no colony could be observed via the plate counting method, and there was no change with the increase in time. *E. coli* is a kind of opportunistic pathogen. Many antibacterial materials have obvious inhibitory effect on *E. coli* [9]. In some silver-loaded antibacterial materials, when the concentration of silver nitrate was 17 g/L, the antibacterial material of 0.8 g/L had a significant antibacterial effect within 1 h in the antibacterial experiment [47]. The results of this study reduced the amount of silver nitrate to 0.5 g/L. In the antibacterial experiment, when the dosage of the complex was 0.2 g/L, it had an antibacterial effect within 1 h.
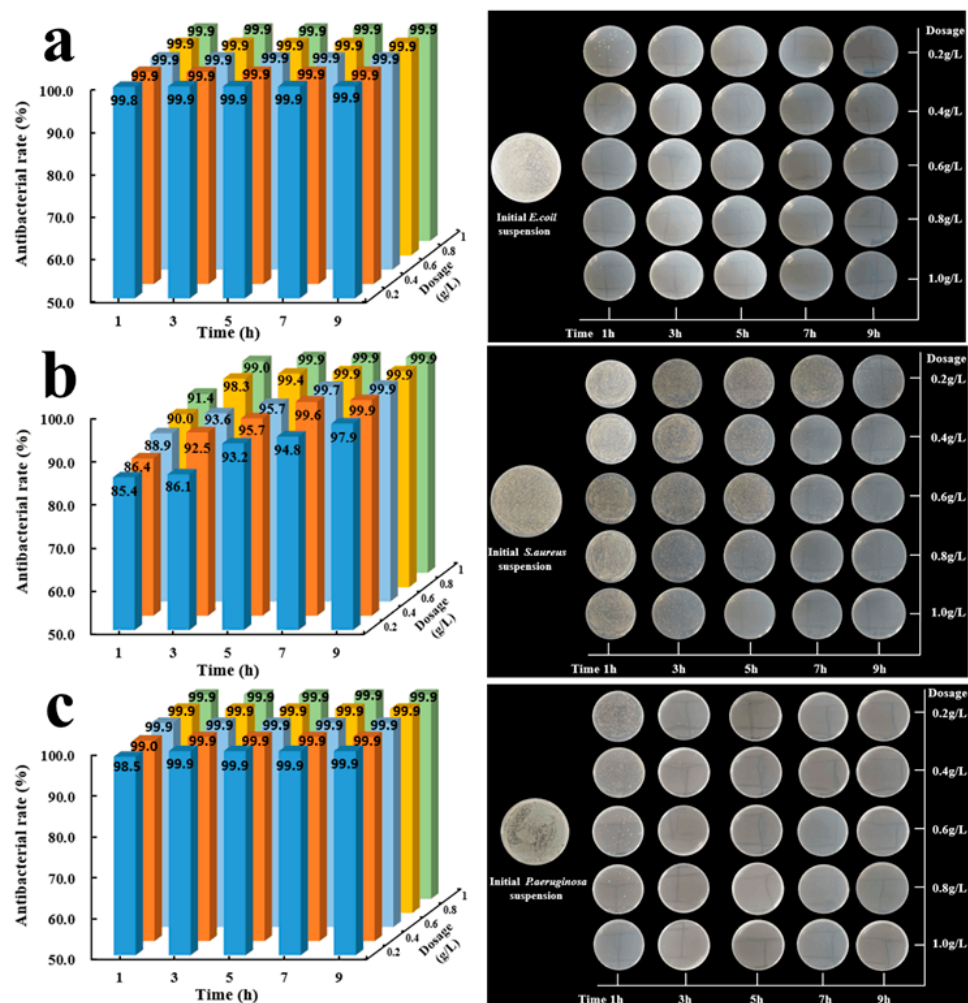
Figure 9. Images of antibacterial effect of the F/C–Ag composite on *E. coli* (**a**), *S. aureus* (**b**) and *P. aeruginosa* (**c**), at different composite dosages and time.

As displayed in Figure 9b, the bacteriostatic activity was tested against *S. aureus*. When the dosage of the F/C–Ag composite was 0.2 g/L and the antibacterial time was 1 h, the antibacterial effect was 85.4%. Plate counting method showed that there were several *S. aureus* colonies on the agar plate. When the duration of the bacteriostatic experiment increased to 9 h, the bacteriostatic rate was 97.9%. The decrease in colony number could be observed through the plate counting method. When the F/C–Ag composite was 0.2 g/L, the bacteriostatic rate increased with increasing performance time, and the number of colonies decreased gradually, as observed via the plate counting method. When the concentration was 1 g/L and the bacteriostasis time was 9 h, there were still some colonies on the agar plate, but the overall bacteriostasis rate was as high as 99.9%. *S. aureus* is a common foodborne pathogenic microorganism, and many research results of antibacterial materials have displayed excellent inhibitory effects. The usual inhibition rate against *S. aureus* was 95% [61]. The antibacterial rate of natural antibacterial materials on *S. aureus* significantly dropped at the same dose [62]. While the amount of silver nitrate used in the biochar materials prepared in our work was low, the antibacterial rate reached 99% after 5 h.

As revealed in Figure 9c, the F/C–Ag composite had excellent antibacterial effect in the antibacterial experiment of *P. aeruginosa*. When the dosage of the F/C–Ag composite material was 0.2 g/L and the antibacterial time was 1 h, the antibacterial effect reached 98.5%. When the time was reached 9 h, no viable colonies could be seen via the plate counting method. After the treatment with the F/C–Ag composite (>0.2 g/L) for 3 h, only a single colony could be seen via the plate counting method. When the concentration

continued to rise to 1 g/L, no residual colonies were found in the plate count. Therefore, for the antibacterial experiment of *E. coli*, the appropriate antibacterial dosage of the F/C–Ag composite was 0.2 g/L, and the optimal antibacterial time was 1 h. In the antibacterial test of *S. aureus*, the optimum bacteriostatic dosage of the F/C–Ag composite was 1 g/L and the optimum bacteriostatic time was 9 h. In the antibacterial experiment of *P. aeruginosa*, the optimal antibacterial dosage of the F/C–Ag composite was 0.2 g/L and the optimal antibacterial time was 3 h. *P. aeruginosa* is one of the most common bacteria present in the soil [63]. The drug resistance of *Pseudomonas* is strong, and thus the antibacterial effect of natural antibacterial materials dropped [64]. The antibacterial properties of nanometal particles were uneven [9]. In the antibacterial test of *P. aeruginosa*, the antibacterial rate reached 99% at the F/C–Ag composite dosage of 0.2 g/L for 3 h. This proves that the composite antibacterial material had a good application prospect.

The antibacterial properties of F/C–Ag composites are closely related to silver ion sterilization [65]. So far, the definitive mechanism of microbial death involving AgNPs is unknown. Figure 10 showed the antibacterial diagram of the F/C–Ag composite. Low-temperature calcination would make the structure of the fish scale loose and the reduced silver nanoparticles might better adhere to the fish scale carbon. The repeatability test verified that the silver nanoparticles were firmly loaded on the composite material. F/C–Ag composites showed good performance in all the antibacterial tests. It proved that substantial AgNPs were released during the antibacterial process. The F/C–Ag composite containing AgNPs released silver ions and diffused them into bacteria through the ion channels. This could be ascribed to their high affinity for biomolecules with sulfur and phosphorus groups present in bacterial membranes [13]. The interaction of AgNPs with mitochondrial respiratory enzymes led to the proliferation of reactive oxygen species, which eventually caused the destruction of ion transport channels and membrane proton gradients, disruption of many cellular metabolic processes (such as DNA synthesis, protein, and enzyme synthesis), and bacterial death [66]. The AgNPs with positive charge had a good antibacterial effect on a wide range of bacteria in the study of silver ion inhibition [59]. According to the results of the antibacterial experiments, it was speculated that there were a lot of positively charged AgNPs in the F/C–Ag composite.
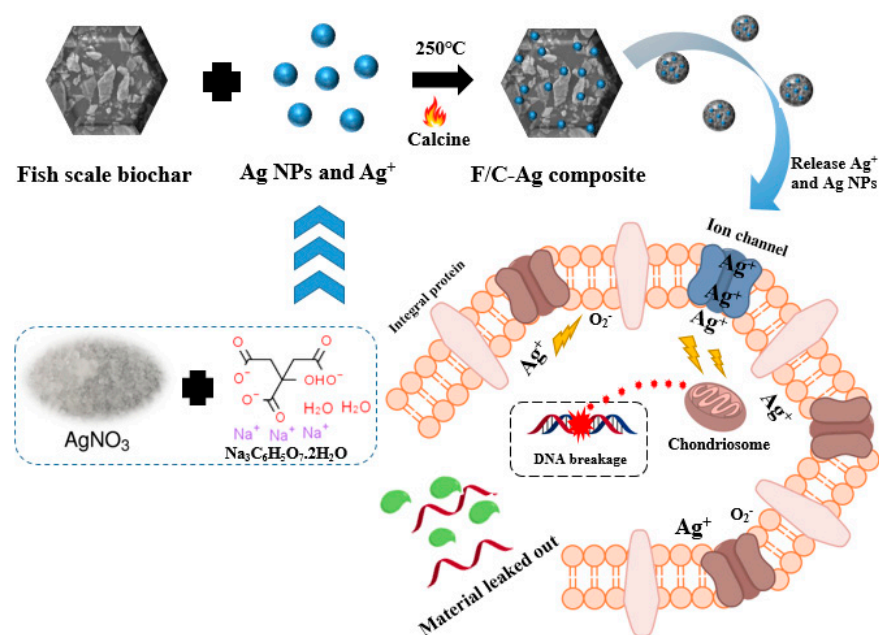

Figure 10. Antibacterial effect of F/C–Ag composites.

Based on the analysis of the characterization results, the fish scale biochar contained a large amount of hydroxyapatite. Some studies showed that hydroxyapatite had a fine texture for loading more metal ions to prepare the antibacterial materials [67]. Using

waste fish scale as raw material, biochar antibacterial materials with excellent antibacterial properties were prepared using low-carbon and environmentally friendly methods. This biochar antibacterial material contained an abundance of silver nanoparticles, and good inhibition rate (99.9%) and excellent reusability (20 times) were obtained. Overall, this biochar antibacterial material had potential application in the future.

3.2.5. Minimum Bacteriostatic Concentration of F/C–Ag Composites

The inhibitory effects of F/C–Ag composites of different concentrations on *E. coli* are displayed in Figure 11a. When the concentration of the F/C–Ag complex was 0.5, 1, 2, 4, and 8 g/L, the OD value tends to be zero. Therefore, when the concentration of the antibacterial material was greater than 0.5 g/L, the growth of *E. coli* was inhibited. When the concentration of the F/C–Ag composite decreased to 0.25 mg/mL, OD value increased sharply, and it increased significantly as the concentration of the F/C–Ag composite continued to decrease. It was concluded that 0.5 mg/mL was the minimum inhibitory concentration of the F/C–Ag composite against *E. coli*. Figure 11b revealed that the inhibitory effect of F/C–Ag composites with different concentrations on *S. aureus*. OD value basically tended to be zero when the concentration of F/C–Ag composites was 1, 2, 4, and 8 g/L, indicating that the growth of *S. aureus* was inhibited under these concentration gradients. When the F/C–Ag composite decreased to 0.5 g/L, OD value increased sharply, and it increased significantly as the concentration of the F/C–Ag composite continued to decrease. It was concluded that the concentration inflection point of 1 g/L was the minimum inhibitory concentration of F/C–Ag composites against *S. aureus*. Figure 11c showed the inhibitory effect of F/C–Ag composites with different concentrations on *P. aeruginosa*. OD value basically tended to be zero when the concentration of F/C–Ag composites was 0.25, 0.5, 1, 2, 4 and 8 g/L, indicating that the growth of *P. aeruginosa* was inhibited under these concentration gradients. When the concentration of the F/C–Ag composite was reduced to 0.125 g/L, the absorbance increased significantly and it continued to increase with the continuous decrease in F/C–Ag composite concentration. It was concluded that 0.25 mg/mL was the minimum inhibitory concentration of F/C–Ag composites against *P. aeruginosa*. Compared with the general biochar antibacterial materials [14], the minimum inhibitory concentration of the F/C–Ag complex could exceed the conventional level.
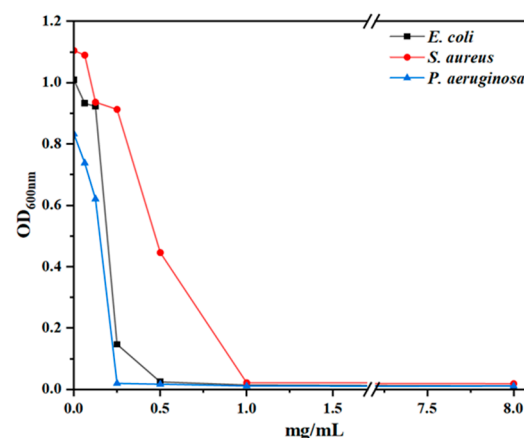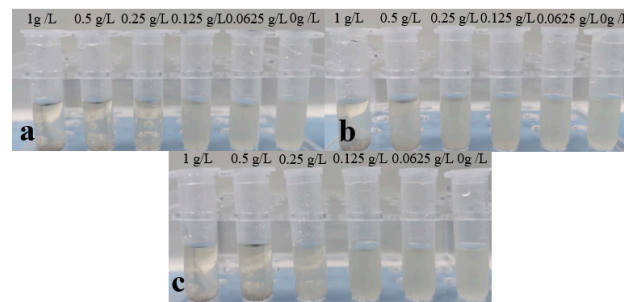

Figure 11. *Cont.*

Figure 11. Minimum inhibitory concentration of *E. coli* (**a**), *S. aureus* (**b**) and *P. aeruginosa* (**c**).

3.3. Antibacterial Reusability

Reusability is a criterion to measure the quality of antibacterial materials [11,68]. Maintaining a high inhibition rate after multiple antibacterial tests would reduce the cost of application. As illustrated in Figure 12, from the repetitions of the *E. coli* bacteriostasis test, the first 15 times had a 100% bacteriostasis effect. After the 16th batch, there was a slight downward trend, and in the 20th time, the bacteriostasis effect became stable, with a bacteriostasis rate of nearly 95%. According to the *S. aureus* bacteriostatic test, when the water bacteriostatic test was repeated for the ninth time, the bacteriostatic effect of the F/C–Ag composite material had a certain downward trend. After the 15th water test, the antibacterial effect leveled off and reached more than 85%. The F/C–Ag composite showed very good bacteriostatic effect and reusability in the experiment of *P. aerugine*. The antibacterial rate in each of the 20 repetitions was 100%. After 20 repeated tests, the antibacterial rates of F/C–Ag composites against three kinds of bacteria were 94.5%, 86.2%, and 100%, respectively. Although the bacteriostatic efficiency dropped slightly with the increasing number of cycles, the bacteriostatic rate against three kinds of bacteria was over 85%, verifying that this biochar composite antibacterial material had good reusability.
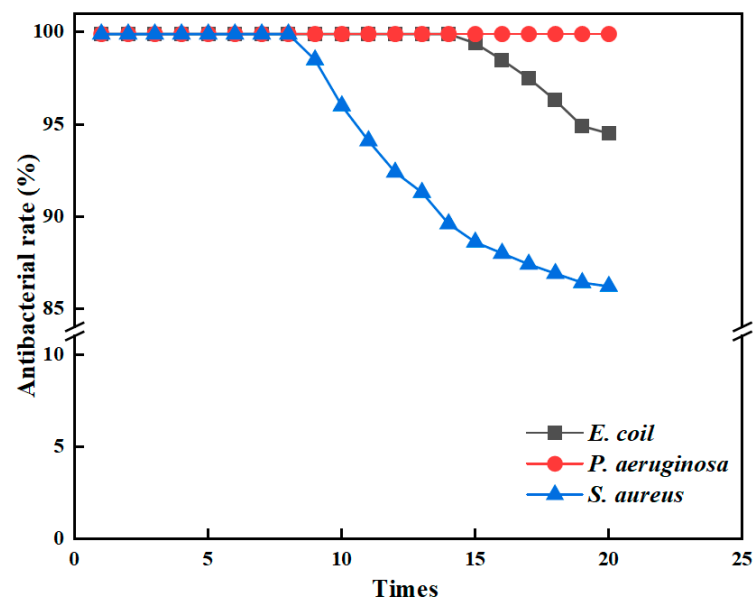

Figure 12. Antibacterial rates with the increase in the number of cycles.

4. Conclusions

The biochar–nanosilver antibacterial composite was prepared with fish scale biochar as substrate and silver nanoparticles as the antibacterial substance. Silver ions were reduced via a simple reduction method, and were fully loaded on the surface of fish scale biochar through low-temperature calcination. The prepared F/C–Ag composites had good antibacterial activity and durability. Moreover, the composites were characterized via

FT-IR, SEM, XRD, XPS, and TG. The method of increasing silver ion loading was studied. F/C–Ag composites showed strong antibacterial ability and good reusability in the antibacterial experiments. The results displayed that the F/C–Ag composite had potential application in the sterilization of drinking water and in the replacement of hydroxyapatite antibacterial materials.

References

1. Xu, J.; Xu, Z. China sewage treatment engineering issues assessment. *J. Clean. Prod.* **2022**, *377*, 134391. [CrossRef]
2. Charles, F.R.; Lim, J.X.; Chen, H.; Goh, S.G.; He, Y.; Gin, K.Y. Prevalence and characterization of antibiotic resistant bacteria in raw community sewage from diverse urban communities. *Sci. Total. Environ.* **2022**, *825*, 153926. [CrossRef] [PubMed]
3. Yang, W.; Cai, C.; Guo, Y.; Wu, H.; Guo, Y.; Dai, X. Diversity and fate of human pathogenic bacteria, fungi, protozoa, and viruses in full-scale sludge treatment plants. *J. Clean. Prod.* **2022**, *380*, 134990. [CrossRef]
4. Haramoto, E.; Kitajima, M.; Hata, A.; Torrey, J.R.; Masago, Y.; Sano, D.; Katayama, H. A review on recent progress in the detection methods and prevalence of human enteric viruses in water. *Water Res.* **2018**, *135*, 168–186. [CrossRef]
5. Ke, X.; Wang, C.; Jing, D.; Zhang, Y.; Zhang, H. Assessing water quality by ratio of the number of dominant bacterium species between surface/subsurface sediments in Haihe River Basin. *Mar. Pollut. Bull.* **2015**, *98*, 267–273. [CrossRef]
6. Luby, S.P.; Halder, A.K.; Huda, T.M.; Unicomb, L.; Islam, M.S.; Arnold, B.F.; Johnston, R.B. Microbiological Contamination of Drinking Water Associated with Subsequent Child Diarrhea. *Am. J. Trop. Med. Hyg.* **2015**, *93*, 904–911. [CrossRef] [PubMed]
7. Noguchi, M.; Aizawa, R.; Nakazawa, D.; Hakumura, Y.; Furuhashi, Y.; Yang, S.; Ninomiya, K.; Takahashi, K.; Honda, R. Application of real treated wastewater to starch production by microalgae: Potential effect of nutrients and microbial contamination. *Biochem. Eng. J.* **2021**, *169*, 107973. [CrossRef]
8. Avcu, E.; Bastan, F.E.; Guney, M.; Yildiran Avcu, Y.; Ur Rehman, M.A.; Boccaccini, A.R. Biodegradable Polymer Matrix Composites Containing Graphene-Related Materials for Antibacterial Applications: A Critical Review. *Acta Biomater.* **2022**, *151*, 1–44. [CrossRef]
9. Mishra, A.; Pradhan, D.; Halder, J.; Biswasroy, P.; Rai, V.K.; Dubey, D.; Kar, B.; Ghosh, G.; Rath, G. Metal nanoparticles against multi-drug-resistance bacteria. *J. Inorg. Biochem.* **2022**, *237*, 111938. [CrossRef]
10. Zhao, X.-Q.; Wahid, F.; Zhao, X.-J.; Wang, F.-P.; Wang, T.-F.; Xie, Y.-Y.; Jia, S.-R.; Zhong, C. Fabrication of amino acid-based supramolecular hydrogel with silver ions for improved antibacterial properties. *Mater. Lett.* **2021**, *300*, 130161. [CrossRef]
11. Zhao, H.; Li, X.; Zhang, L.; Hu, Z.; Zhong, L.; Xue, J. Preparation and bacteriostatic research of porous polyvinyl alcohol/biochar/nanosilver polymer gel for drinking water treatment. *Sci. Rep.* **2021**, *11*, 12205. [CrossRef]
12. Zhang, L.; Zheng, S.; Hu, Z.; Zhong, L.; Wang, Y.; Zhang, X.; Xue, J. Preparation of Polyvinyl Alcohol/Bacterial-Cellulose-Coated Biochar–Nanosilver Antibacterial Composite Membranes. *Appl. Sci.* **2020**, *10*, 752. [CrossRef]
13. Abbaszadegan, A.; Ghahramani, Y.; Gholami, A.; Hemmateenejad, B.; Dorostkar, S.; Nabavizadeh, M.; Sharghi, H. The Effect of Charge at the Surface of Silver Nanoparticles on Antimicrobial Activity against Gram-Positive and Gram-Negative Bacteria: A Preliminary Study. *J. Nanomater.* **2015**, *2015*, 720654. [CrossRef]
14. Abdelwahab, M.S.; El Halfawy, N.M.; El-Naggar, M.Y. Lead adsorption and antibacterial activity using modified magnetic biochar/sodium alginate nanocomposite. *Int. J. Biol. Macromol.* **2022**, *206*, 730–739. [CrossRef]
15. Zha, J.; Fan, B.; He, J.; He, Y.C.; Ma, C. Valorization of biomass to furfural by chestnut shell-based solid acid in methyl isobutyl ketone-water-sodium chloride system. *Appl. Biochem. Biotechnol.* **2022**, *194*, 2021–2035. [CrossRef] [PubMed]
16. Ji, L.; Tang, Z.; Yang, D.; Ma, C.; He, Y.C. Improved one-pot synthesis of furfural from corn stalk with heterogeneous catalysis using corn stalk as biobased carrier in deep eutectic solvent-water system. *Bioresour. Technol.* **2021**, *340*, 125691. [CrossRef]

17. Gong, L.; Zha, J.; Pan, L.; Ma, C.; He, Y.C. Highly efficient conversion of sunflower stalk-hydrolysate to furfural by sunflower stalk residue-derived carbonaceous solid acid in deep eutectic solvent/organic solvent system. *Bioresour. Technol.* **2022**, *351*, 126945. [CrossRef] [PubMed]

18. Shen, J.; Gao, R.; He, Y.C.; Ma, C. Efficient synthesis of furfural from waste biomasses by sulfonated crab shell-based solid acid in a sustainable approach. *Ind. Crops Prod.* **2023**, *202*, 116989. [CrossRef]

19. Li, Q.; Di, J.; Liao, X.; Ni, J.; Li, Q.; He, Y.C.; Ma, C. Exploration of benign deep eutectic solvent–water systems for the highly efficient production of furfurylamine from sugarcane bagasse via chemoenzymatic cascade catalysis. *Green Chem.* **2021**, *23*, 8154–8168. [CrossRef]

20. Ni, J.; Li, Q.; Gong, L.; Liao, X.L.; Zhang, Z.J.; Ma, C.; He, Y. Highly efficient chemoenzymatic cascade catalysis of biomass into furfurylamine by a heterogeneous shrimp shell-based chemocatalyst and an ω-transaminase biocatalyst in deep eutectic solvent—Water. *ACS Sustain. Chem. Eng.* **2021**, *9*, 13084–13095. [CrossRef]

21. Yi, L.; Zuo, L.; Wei, C.; Fu, H.; Qu, X.; Zheng, S.; Xu, Z.; Guo, Y.; Li, H.; Zhu, D. Enhanced adsorption of bisphenol A, tylosin, and tetracycline from aqueous solution to nitrogen-doped multiwall carbon nanotubes via cation-pi and pi-pi electron-donor-acceptor (EDA) interactions. *Sci. Total. Environ.* **2020**, *719*, 137389. [CrossRef] [PubMed]

22. Ye, Y.; Barange, M.; Beveridge, M.; Garibaldi, L.; Gutierrez, N.; Anganuzzi, A.; Taconet, M. FAO's statistic data and sustainability of fisheries and aquaculture: Comments on Pauly and Zeller (2017). *Mar. Policy* **2017**, *81*, 401–405. [CrossRef]

23. Ikoma, T.; Kobayashi, H.; Tanaka, J.; Walsh, D.; Mann, S. Microstructure, mechanical, and biomimetic properties of fish scales from Pagrus major. *J. Struct. Biol.* **2003**, *142*, 327–333. [CrossRef]

24. Greggio, N.; Serafini, A.; Balugani, E.; Carlini, C.; Contin, A.; Marazza, D. Quantification and mapping of fish waste in retail trade and restaurant sector: Experience in Emilia-Romagna, Italy. *Waste Manag.* **2021**, *135*, 256–266. [CrossRef]

25. Sar, T.; Ferreira, J.A.; Taherzadeh, M.J. Bioprocessing strategies to increase the protein fraction of Rhizopus oryzae biomass using fish industry sidestreams. *Waste Manag.* **2020**, *113*, 261–269. [CrossRef] [PubMed]

26. Chowdhury, P.; Viraraghavan, T.; Srinivasan, A. Biological treatment processes for fish processing wastewater—A review. *Bioresour. Technol.* **2010**, *101*, 439–449. [CrossRef]

27. Lopes, C.; Antelo, L.T.; Franco-Uria, A.; Alonso, A.A.; Perez-Martin, R. Valorisation of fish by-products against waste management treatments—Comparison of environmental impacts. *Waste Manag.* **2015**, *46*, 103–112. [CrossRef]

28. Qin, D.; Bi, S.; You, X.; Wang, M.; Cong, X.; Yuan, C.; Yu, M.; Cheng, X.; Chen, X.-G. Development and application of fish scale wastes as versatile natural biomaterials. *Chem. Eng. J.* **2022**, *428*, 131102. [CrossRef]

29. Song, F.; Zhao, Q.; Zhu, T.; Bo, C.; Zhang, M.; Hu, L.; Zhu, X.; Jia, P.; Zhou, Y. Biobased coating derived from fish scale protein and phytic acid for flame-retardant cotton fabrics. *Mater. Des.* **2022**, *221*, 110925. [CrossRef]

30. Li, Y.; Shan, P.; Yu, F.; Li, H.; Peng, L. Fabrication and characterization of waste fish scale-derived gelatin/sodium alginate/carvacrol loaded ZIF-8 nanoparticles composite films with sustained antibacterial activity for active food packaging. *Int. J. Biol. Macromol.* **2023**, *230*, 123192. [CrossRef]

31. Fu, B.; Mei, S.; Su, X.; Chen, H.; Zhu, J.; Zheng, Z.; Lin, H.; Dai, C.; Luque, R.; Yang, D.P. Integrating waste fish scale-derived gelatin and chitosan into edible nanocomposite film for perishable fruits. *Int. J. Biol. Macromol.* **2021**, *191*, 1164–1174. [CrossRef]

32. Han, F.; Li, T.; Li, M.; Zhang, B.; Wang, Y.; Zhu, Y.; Wu, C. Nano-calcium silicate mineralized fish scale scaffolds for enhancing tendon-bone healing. *Bioact. Mater.* **2023**, *20*, 29–40. [CrossRef]

33. Yamaura, K.; Mifune, Y.; Inui, A.; Nishimoto, H.; Mukohara, S.; Yoshikawa, T.; Shinohara, I.; Kato, T.; Furukawa, T.; Hoshino, Y.; et al. Novel therapy using a fish scale collagen scaffold for rotator cuff healing in rat models. *J. Shoulder Elb. Surg.* **2022**, *31*, 2629–2637. [CrossRef]

34. Xia, Y.; Meng, F.; Wang, S.; Li, P.; Geng, C.; Zhang, X.; Zhou, Z.; Kong, F. Tough, antibacterial fish scale gelatin/chitosan film with excellent water vapor and UV-blocking performance comprising liquefied chitin and silica sol. *Int. J. Biol. Macromol.* **2022**, *222*, 3250–3260. [CrossRef] [PubMed]

35. Masilan, K.; Neethiselvan, N.; Shakila, R.J.; Muralidharan, N.; Karthy, A.; Ravikumar, T.; Parthiban, F. Investigation on the coacervation of fish scale gelatin hydrogel with seafood waste hydrolysates for the development of artificial fish bait: Physico-chemical, thermodynamic, and morpho-structural properties. *J. Indian. Chem. Soc.* **2022**, *99*, 100783. [CrossRef]

36. Deng, J.-J.; Mao, H.-H.; Fang, W.; Li, Z.-Q.; Shi, D.; Li, Z.-W.; Zhou, T.; Luo, X.-C. Enzymatic conversion and recovery of protein, chitin, and astaxanthin from shrimp shell waste. *J. Clean. Prod.* **2020**, *271*, 122655. [CrossRef]

37. Li, S.; Chi, S.; Lin, C.; Cai, C.; Yang, L.; Peng, K.; Huang, X.; Liu, J. Combination of biochar and AMF promotes phosphorus utilization by stimulating rhizosphere microbial co-occurrence networks and lipid metabolites of Phragmites. *Sci. Total. Environ.* **2022**, *845*, 157339. [CrossRef] [PubMed]

38. Wang, J.; Liang, J.; Sun, L.; Shen, J.; He, Z. Enhancing anammox resistance to low operating temperatures with the use of PVA gel beads. *Sci. Total. Environ.* **2021**, *774*, 144826. [CrossRef]

39. Zhu, Q.; Liu, X.; Hao, T.; Zeng, M.; Shen, J.; Zhang, F.; De Vries, W. Modeling soil acidification in typical Chinese cropping systems. *Sci. Total. Environ.* **2018**, *613–614*, 1339–1348. [CrossRef]

40. Pezeshkpour, V.; Khosravani, S.A.; Ghaedi, M.; Dashtian, K.; Zare, F.; Sharifi, A.; Jannesar, R.; Zoladl, M. Ultrasound assisted extraction of phenolic acids from broccoli vegetable and using sonochemistry for preparation of MOF-5 nanocubes: Comparative study based on micro-dilution broth and plate count method for synergism antibacterial effect. *Ultrason. Sonochem* **2018**, *40*, 1031–1038. [CrossRef]

41. Balouiri, M.; Sadiki, M.; Ibnsouda, S.K. Methods for in vitro evaluating antimicrobial activity: A review. *J. Pharm. Anal.* **2016**, *6*, 71–79. [CrossRef]

42. Wu, J.; Zhang, G.; Liu, J.; Gao, H.; Song, C.; Du, H.; Zhang, L.; Gong, Z.; LÜ, Y. Synthesis, characteristics, and antibacterial activity of a rare-earth samarium/silver/titanium dioxide inorganic nanomaterials. *J. Rare Earths* **2014**, *32*, 727–732. [CrossRef]

43. Hadder, B.; Dexter, F.; Robinson, A.D.M.; Loftus, R.W. Molecular characterisation and epidemiology of transmission of intraoperative *Staphylococcus aureus* isolates stratified by vancomycin minimum inhibitory concentration (MIC). *Infect. Prev. Pr.* **2022**, *4*, 100249. [CrossRef]

44. Xu, Y.; Tan, L.; Li, Q.; Zheng, X.; Liu, W. Sublethal concentrations of heavy metals Cu^{2+} and Zn^{2+} can induce the emergence of bacterial multidrug resistance. *Environ. Technol. Innov.* **2022**, *27*, 102379. [CrossRef]

45. Shi, N.; Gao, Y.; Yin, D.; Song, Y.; Kang, J.; Li, X.; Zhang, Z.; Feng, X.; Duan, J. The effect of the sub-minimal inhibitory concentration and the concentrations within resistant mutation window of ciprofloxacin on MIC, swimming motility and biofilm formation of Pseudomonas aeruginosa. *Microb. Pathog.* **2019**, *137*, 103765. [CrossRef] [PubMed]

46. Zhang, L.; Bai, X.; Tian, H.; Zhong, L.; Ma, C.; Zhou, Y.; Chen, S.; Li, D. Synthesis of antibacterial film CTS/PVP/TiO_2/Ag for drinking water system. *Carbohydr. Polym.* **2012**, *89*, 1060–1066. [CrossRef]

47. Hu, Z.; Zhang, L.; Zhong, L.; Zhou, Y.; Xue, J.; Li, Y. Preparation of an antibacterial chitosan-coated biochar-nanosilver composite for drinking water purification. *Carbohydr. Polym.* **2019**, *219*, 290–297. [CrossRef] [PubMed]

48. Barakat, N.A.M.; Khil, M.S.; Omran, A.M.; Sheikh, F.A.; Kim, H.Y. Extraction of pure natural hydroxyapatite from the bovine bones bio waste by three different methods. *J. Mater. Process. Technol.* **2009**, *209*, 3408–3415. [CrossRef]

49. Xia, D.; Liu, Y.; Cheng, X.; Gu, P.; Chen, Q.; Zhang, Z. Temperature-tuned fish-scale biochar with two-dimensional homogeneous porous structure: A promising uranium extractant. *Appl. Surf. Sci.* **2022**, *591*, 153136. [CrossRef]

50. Kiran, J.U.; Roners, J.P.; Mathew, S. XPS and thermal studies of silver doped SiO_2 matrices for plasmonic applications. *Mater. Today Proc.* **2020**, *33*, 1263–1267. [CrossRef]

51. Larrabure, G.; Chero-Osorio, S.; Silva-Quiñones, D.; Benndorf, C.; Williams, M.; Gao, F.; Gamarra, C.; Alarcón, A.; Segura, C.; Teplyakov, A.; et al. Surface processes at a polymetallic (Mn-Fe-Pb) sulfide subject to cyanide leaching under sonication conditions and with an alkaline pretreatment: Understanding differences in silver extraction with X-ray photoelectron spectroscopy (XPS). *Hydrometallurgy* **2021**, *200*, 105544. [CrossRef]

52. Hosny, M.; Fawzy, M.; Eltaweil, A.S. Phytofabrication of bimetallic silver-copper/biochar nanocomposite for environmental and medical applications. *J. Environ. Manag.* **2022**, *316*, 115238. [CrossRef] [PubMed]

53. Panda, N.N.; Pramanik, K.; Sukla, L.B. Extraction and characterization of biocompatible hydroxyapatite from fresh water fish scales for tissue engineering scaffold. *Bioprocess Biosyst. Eng.* **2014**, *37*, 433–440. [CrossRef]

54. Zhou, Y.; Gao, B.; Zimmerman, A.R.; Cao, X. Biochar-supported zerovalent iron reclaims silver from aqueous solution to form antimicrobial nanocomposite. *Chemosphere* **2014**, *117*, 801–805. [CrossRef]

55. Cui, J.; Liang, Y.; Yang, D.; Liu, Y. Facile fabrication of rice husk based silicon dioxide nanospheres loaded with silver nanoparticles as a rice antibacterial agent. *Sci. Rep.* **2016**, *6*, 21423. [CrossRef] [PubMed]

56. Saha, S.; Malik, M.M.; Qureshi, M.S. Study of Synergistic Effects of Antibiotics And Triangular Shaped Silver Nanoparticles, Synthesized Using UV-Light Irradiation, on *S. aureus* and *P. aeruginosa*. *Mater. Today Proc.* **2019**, *18*, 920–927. [CrossRef]

57. Mathivanan, K.; Selva, R.; Chandirika, J.U.; Govindarajan, R.K.; Srinivasan, R.; Annadurai, G.; Duc, P.A. Biologically synthesized silver nanoparticles against pathogenic bacteria: Synthesis, calcination and characterization. *Biocatal. Agric. Biotechnol.* **2019**, *22*, 101373. [CrossRef]

58. Tripathi, D.K.; Tripathi, A.; Shweta; Singh, S.; Singh, Y.; Vishwakarma, K.; Yadav, G.; Sharma, S.; Singh, V.K.; Mishra, R.K.; et al. Uptake, Accumulation and Toxicity of Silver Nanoparticle in Autotrophic Plants, and Heterotrophic Microbes: A Concentric Review. *Front. Microbiol.* **2017**, *8*, 7. [CrossRef]

59. Gebauer, J.S.; Treuel, L. Influence of individual ionic components on the agglomeration kinetics of silver nanoparticles. *J. Colloid. Interface Sci.* **2011**, *354*, 546–554. [CrossRef]

60. Huang, J.-F.; Shi, Q.-S.; Feng, J.; Chen, M.-J.; Li, W.-R.; Li, L.-Q. Facile pyrolysis preparation of rosin-derived biochar for supporting silver nanoparticles with antibacterial activity. *Compos. Sci. Technol.* **2017**, *145*, 89–95. [CrossRef]

61. Zhao, Y.; Wei, J.; Li, C.; Ahmed, A.F.; Liu, Z.; Ma, C. A comprehensive review on mechanism of natural products against Staphylococcus aureus. *J. Future Foods* **2022**, *2*, 25–33. [CrossRef]

62. Troïa, T.; Siad, J.; Di Giorgio, C.; Brunel, J.M. Design and synthesis of new polyamine quinoline antibiotic enhancers to fight resistant gram-negative *P. aeruginosa* bacteria. *Eur. J. Med. Chem. Rep.* **2022**, *5*, 100054. [CrossRef]

63. Diaz Santos, E.; Mora Jimenez, C.; Del Rio-Carbajo, L.; Vidal-Cortes, P. Treatment of severe multi-drug resistant Pseudomonas aeruginosa infections. *Med. Intensiv.* **2022**, *46*, 508–520. [CrossRef]

64. Ahmed, B.; Hashmi, A.; Khan, M.S.; Musarrat, J. ROS mediated destruction of cell membrane, growth and biofilms of human bacterial pathogens by stable metallic AgNPs functionalized from bell pepper extract and quercetin. *Adv. Powder Technol.* **2018**, *29*, 1601–1616. [CrossRef]

65. Velidandi, A.; Pabbathi, N.P.P.; Dahariya, S.; Baadhe, R.R. Green synthesis of novel Ag–Cu and Ag–Znbimetallic nanoparticles and their in vitro biological, eco-toxicity and catalytic studies. *Nano-Struct. Nano-Objects* **2021**, *26*, 100687. [CrossRef]

66. Aryan, N.; Behpour, M.; Benvidi, A.; Kashi, F.J.; Azimzadeh, M.; Zare, H.R. Evaluation of sodium alendronate drug released from TiO$_2$ nanoparticle doped with hydroxyapatite and silver–strontium for enhancing antibacterial effect and osteoinductivity. *Mater. Chem. Phys.* **2023**, *295*, 126934. [CrossRef]
67. Yang, D.; Gong, L.; Li, Q.; Fan, B.; Ma, C.; He, Y. Preparation of a biobased polyelectrolyte complex from chitosan and sodium carboxymethyl cellulose and its antibacterial characteristics. *Int. J. Biol. Macromol.* **2023**, *227*, 524–534. [CrossRef]
68. Sarojini, S.; Vanathi Vijayalakshmi, R. XPS studies on silver ion conducting solid electrolyte SbI3-Ag2MoO4. Mater. *Today Proc.* **2022**, *68*, 314–318. [CrossRef]